Editors' Suggestion | Featured in Physics

How the zebra got its stripes: Curvature-dependent diffusion orients Turing patterns on three-dimensional surfaces

Michael F. Staddon
Center for Systems Biology Dresden, Dresden 01307, Germany;
Max Planck Institute for the Physics of Complex Systems, Dresden 01187, Germany;
and Max Planck Institute of Molecular Cell Biology and Genetics, Dresden 01307, Germany

(Received 4 December 2023; accepted 18 July 2024; published 3 September 2024)

Many animals have patterned fur, feathers, or scales, such as the stripes of a zebra. Turing models, or reaction-diffusion systems, are a class of mathematical models of interacting species that have been successfully used to generate animal-like patterns for many species. When diffusion of the inhibitor is high enough relative to the activator, a diffusion-driven instability can spontaneously form patterns. However, it is not just the type of pattern but also the orientation that matters, and it remains unclear how patterns are oriented in practice. Here, we propose a mechanism by which the curvature of the surface influences the rate of diffusion, and can recapture the correct orientation of stripes on models of a zebra and of a cat in numerical simulations. Previous work has shown how anisotropic diffusion can give stripe forming reaction-diffusion systems a bias in orientation. From the observation that zebra stripes run around the direction of highest curvature, that is around the torso and legs, we apply this result by modifying the anisotropic diffusion rates based on the local curvature. These results show how local geometry can influence the reaction dynamics to give robust, global-scale patterns. Overall, this model proposes a coupling between the system geometry and reaction-diffusion dynamics that can give global control over the patterning by using only local curvature information. Such a model can give shape and positioning information in animal development without the need for spatially dependent morphogen gradients.

DOI: 10.1103/PhysRevE.110.034402

I. INTRODUCTION

Many animals have patterned fur, feathers, or scales that can serve many different purposes, such as the camouflaging stripes of a tiger or zebra, sexual selection as in the peacocks feathers, or as a warning signal in striped venomous snakes or caterpillars. For striped patterns, it can be important that the stripes are oriented in a specific manner for effective function. A tiger with horizontal stripes might stick out from the vertical blades of grass and fail to sneak up on its prey. Often the orientation depends on the location on the body. For a standing tiger or zebra, stripes are aligned vertically around the torso and horizontally around the legs. The width of the stripes can vary too. For zebras, stripes can be three to five times thinner around the legs compared to the torso [1], and animals like giraffes and leopards have smaller spots around their legs compared to their torso [2], or the spots elongating into stripes around the legs and tails as in some tabby or Bengal cats. However, it remains unclear how these patterns are arranged during development.

Alan Turing famously proposed a model for pattern formation [3], now known as Turing models or reaction-diffusion models. Typically there are two interacting and diffusing species which, under the right conditions, can produce periodic patterns known as Turing patterns from an initially uniform state due to a diffusion-driven instability [3–6]. There has been theoretical success in reproducing a wide range of animal pigmentation patterns [7–11], digit formation in hands and feet [12,13], and hair and feather positioning [14,15], with some experimental evidence of biological circuits that could act as Turing models [7,9,14–16].

However, standard Turing models generate patterns with no bias in orientation while in nature these patterns are often aligned in specific directions. One argument is that the geometry of the animal may limit waves to certain directions. For example, the wavelength of stripes on a tigers tail may be larger than the tails circumference, and so patterns may only emerge with stripes going around the tail [4,17,18]. However, this argument clearly breaks down when looking at the animals torso which often have vertical stripes with a wavelength much smaller than the radius of curvature. Instead, there are several additional mechanisms that can orient Turing-like patterns [19]. Including spatial gradients of chemical source in the reaction rates can align stripes, either perpendicular or parallel to the gradient, depending which species the chemical source affects [8,11,12,20]. Alternatively, anisotropic diffusion [21,22] or anisotropic growth of the domain [23] can also lead to stripe orientation.

In this paper, we present a theoretical mechanism for aligning Turing patterns that reproduces the orientations observed in tigers and zebras. In zebras and tigers, the stripes go around the legs and torso, which is in the direction of highest curvature. Thus, we propose a model for pattern alignment in

which the diffusion is coupled to the curvature of the surface. While anisotropic curvature differentiates directions through the Laplacian and can produce pattern alignment when curvature is high [4,23,24], meaning the diffusion coefficient curvature dependent can boost this effect when curvature is low, such as on the torso, or even reverse the effects. Additionally, when patterns are established early in embryonic development [25], curvatures are much higher compared to the adult organism, thus any effects from curvature or curvature coupling are much stronger.

First, we review the conditions for Turing instabilities and show analytically that they grow fastest in the direction of highest diffusion of the inhibitor. Next, we show numerically that even for small differences in diffusion we obtain robust alignment of stripes, and how diffusion can transition a spot pattern to stripes. Finally, we perform simulations on 3D models of cats and zebras and show that we can obtain patterns qualitatively similar to those in nature.

II. INSTABILITY AND WAVELENGTHS INCREASE WITH INHIBITOR DIFFUSION

First, we review the conditions for Turing instability and show how increasing the inhibitor diffusion rate increases the growth rate of instabilities. Consider a general two-species reaction-diffusion system [3] with isotropic diffusion

$$\dot{u} = \nabla^2 u + f(u, v), \tag{1}$$

$$\dot{v} = d\nabla^2 v + g(u, v), \tag{2}$$

where f and g are the chemical reaction rates, and d is the relative diffusion rate between v and u, working in nondimensional space. The system has a uniform steady state when $u = u_*$ and $v = v_*$. By considering small perturbations to this steady state of the form $u = u_* + \tilde{u}e^{i(k_x x + k_y y)}$ and $v = v_* + \tilde{v}e^{i(k_x x + k_y y)}$ and using linear stability analysis, one can show that the conditions for Turing instabilities are

(i) $f_u + g_v < 0$,
(ii) $f_u g_v - f_v g_u > 0$,
(iii) $df_u + g_v > 0$,
(iv) $(df_u + g_v)^2 - 4d(f_u g_v - f_v g_u) > 0$,

where $f_u = \partial_u f(u_*, v_*)$, and so on [3]. When these conditions hold, there exists some perturbation with frequency $k = \sqrt{k_x^2 + k_y^2}$ that is linearly unstable and patterns should spontaneously form. The first two conditions are for a steady uniform state and the last two conditions are for a diffusion-drive instability. A corollary of conditions (i) and (iii) is that $d \neq 1$, and further, if $f_u > 0 \Rightarrow d > 1$ and $f_u < 0 \Rightarrow d < 1$, meaning we must have a relatively slow diffusing activator and fast moving inhibitor for patterns to form.

When u is the activator with $f_u > 0$, the maximum growth rate across all frequencies k is given by

$$\lambda(k_*) = \frac{1}{2}\left((f_u + g_v) + \frac{d+1}{d-1}(f_u - g_v) - \frac{4d}{d-1}\sqrt{-\frac{f_v g_u}{d}}\right) \tag{3}$$

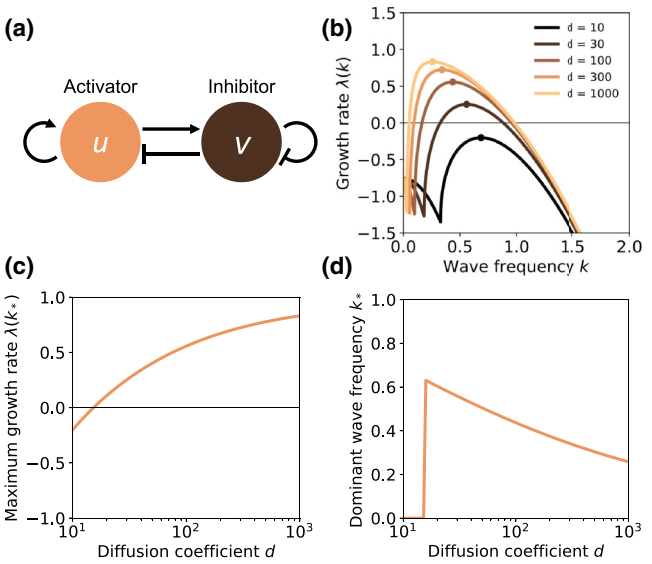

FIG. 1. Inhibitor diffusion increases instabilities. (a) Example two-species reaction diffusion system. The activator u increases production of both u and v while the inhibitor v decreases production. (b) Instability growth rate λ against frequency k for different diffusion coefficients d. (c) Maximum growth rate across all wave numbers against diffusion coefficient d. (d) The dominant frequency k_*, which maximises the growth rate, against diffusion coefficient d.

with corresponding frequency

$$k_* = \sqrt{-\frac{f_u - g_v}{d-1} + \frac{d+1}{d-1}\sqrt{-\frac{f_v g_u}{d}}}. \tag{4}$$

The growth rate always increases with an increase in the diffusion coefficient, as the derivative

$$\partial_d \lambda(k_*) = \frac{1}{2(d-1)^2}\left(-(f_u - g_v) + (d+1)\sqrt{-\frac{f_v g_u}{d}}\right) \tag{5}$$

is always positive since it is proportional to $k_*^2 > 0$, in the case that $f_u > 0$. Similarly, when $f_u < 0$ the derivative is negative, meaning that increasing the relative diffusion rate of the inhibitor increases the instability. Further, for d large enough, the frequency k_* always decreases, meaning that further increases to the diffusion rate increase the pattern wavelength.

To illustrate this result, we use the Schnakenberg model [26] which can produce striped or spotted patterns, depending on the reaction parameters, though these results should hold for any reaction-diffusion system satisfying the Turing conditions. The rate equations are given by

$$\dot{u} = \nabla^2 u + a + u^2 v - u, \tag{6}$$

$$\dot{v} = d\nabla^2 v + b - u^2 v, \tag{7}$$

such that $f(u, v) = a + u^2 v - u$ and $g(u, v) = b - u^2 v$, and has steady state given by $u_* = a + b$ and $v_* = \frac{b}{(a+b)^2}$. In these equations, u is the activator and v is the inhibitor [Fig. 1(a)]. Using the parameters $a = 0.025$ and $b = 1.55$, the diffusion coefficient for the inhibitor must be higher than that of the activator for instabilities to occur, as expected by condition (iii). Once the system is unstable, increasing d further increases the

growth rate of the instabilities [Figs. 1(b) and 1(c)], and the most unstable wave frequency decreases [Fig. 1(d)], giving wider stripes.

III. ANISTROPIC DIFFUSION ALIGNS TURING PATTERNS

Next, we show that anisotropic diffusion should give pattern alignment in unstable systems. Consider a reaction-diffusion system with anisotropic diffusion

$$\dot{u} = \partial_x^2 u + \partial_y^2 u + f(u, v), \tag{8}$$

$$\dot{v} = d_x \partial_x^2 v + d_y \partial_y^2 v + g(u, v). \tag{9}$$

Writing the wave vector of the perturbation as $(k_x, k_y) = (k\cos\theta, k\sin\theta)$ converts our equations into the form discussed in the previous section, except we have an angle-dependent diffusion coefficient $d(\theta) = d_x \cos^2\theta + d_y \sin^2\theta$. From the previous section, increasing the diffusion coefficient increases the instability when the system is unstable. Thus, we expect waves to form in the direction that maximizes $d(\theta)$, and so stripes should form in the perpendicular direction. In addition, it is possible for the perturbation to be stable in one direction and unstable perpendicular to it [22]. Thus, in cases where we have anisotropic diffusion, we expect stripes to align either parallel or perpendicular to the direction of highest diffusion.

To test these predictions, we simulate the Schnakenberg equations in a periodic two-dimensional box with anisotropic diffusion in the inhibitor. We use the parameters $a = 0.025$ and $b = 1.55$, and $d_y = 20$, which would normally give stripes, and vary the diffusion coefficient in the x direction from $d_x = 0.5d_y$ to $d_x = 2d_y$. Starting from the uniform steady state, we add a small perturbation and evolve the system numerically until a steady state is reached.

When $d_x = d_y$ we obtain striped patterns with no bias in orientation [Fig. 2(a), middle panel]. When $d_x < d_y$, stripes align with the x direction, even for differences in diffusion as small as $d_x = 0.93d_y$ [Fig. 2(a), left panels]. Similarly, when $d_x > d_y$ stripes align with the y direction instead [Fig. 2(a), right panel].

For a different set of parameters, $a = 0.025$, $b = 1.24$, $d_x = d_y = 20$, the Schnakenberg equations give a spot pattern instead of stripes [Fig. 2(b), middle panel]. However, as we vary diffusion in the x direction as before we observe a spot to stripe transition. For moderate anisotropy, spots form but begin to be aligned in rows, reminiscent of the rare spotted zebra mutant, which has stripes broken up into spots. At high diffusion anisotropy we observe stripes aligned as before, but for near isotropic diffusion we observe spots [Fig. 2(b)]. Thus, anisotropic diffusion can change both the orientation and type of patterns, depending on the parameter regime of the underlying reaction model.

We quantify pattern alignment by measuring the gradient fraction in the i direction as

$$G_i = \frac{\int \partial_i u^2 dA}{\int (\partial_x u^2 + \partial_y u^2) dA} \tag{10}$$

for $i = x, y$, which measures the fraction of the gradient in a given direction. For $d_x = d_y$ there is no clear preference in pattern direction [Fig. 2(c)], as shown in other studies [27]. However, for $d_x < d_y$ most of the gradient is in the y direction and for $d_x > d_y$ most of the gradient is in the x direction [Fig. 2(c)]. The same trend is observed with the spot forming parameters, although a larger diffusion-anisotropy is needed before patterns align [Fig. 2(d)].

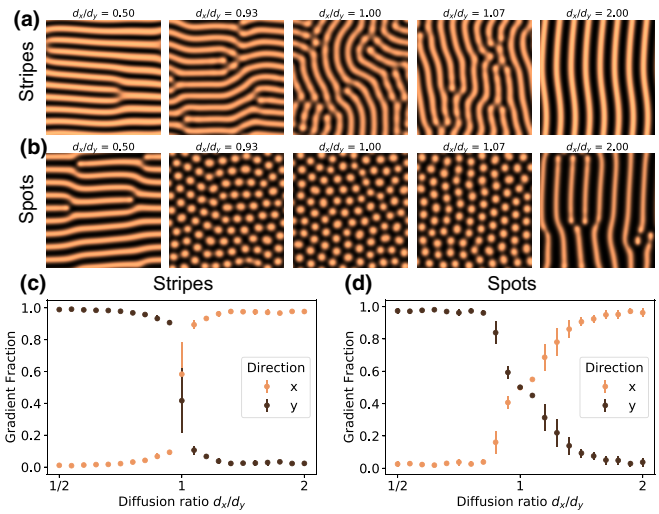

FIG. 2. Anisotropic diffusion gives robust pattern alignment. (a), (b) Simulation results of the Schnakenberg equations for varying ratios of d_x/d_y, where $d_y = 20$, using (a) stripe forming parameters ($a = 0.025$, $b = 1.55$) and (b) spot forming parameters ($a = 0.025$, $b = 1.24$). (c), (d) Gradient fraction in the x and y directions against the diffusion ratio for (c) stripe forming parameters and (d) spot forming parameters. Dots show the mean and standard deviation ($n = 10$).

IV. CURVATURE-DEPENDENT DIFFUSION REPRODUCES ANIMAL PATTERNS

Finally, we introduce the idea of curvature-diffusion coupling and show how it can predict both pattern alignment and wavelengths. We have seen in the previous section how small changes in diffusion with direction can align stripes. Biologically, this could arise from morphogens diffusing on the apical or basal sides of a cell, which would travel different distances when the surfaces are curved [28]. Alternatively, cells shapes can display strong anisotropy around the torso or limbs [29], which could change the diffusion rate in the direction aligned or perpendicular to the cells. Thus, we allow diffusion to be modified by the curvature of a surface in 3D and find that we can qualitatively reproduce the observed patterns.

On a surface in 3D, we have the surface normal $\mathbf{n}$, and two directions of principal directions $\mathbf{t}_1$ and $\mathbf{t}_2$, with curvatures κ_1 and κ_2, respectively. We modify the diffusion of the inhibitor v to be anisotropic and curvature dependent, giving equations

$$\dot{u} = \nabla_S^2 u + f(u, v), \tag{11}$$

$$\dot{v} = \nabla_S \cdot [(d(\kappa_1)\mathbf{t}_1 \otimes \mathbf{t}_1 + d(\kappa_2)\mathbf{t}_2 \otimes \mathbf{t}_2) \cdot \nabla_S v] + g(u, v), \tag{12}$$

where ∇_S is the surface gradient, and $d(\kappa)$ is a curvature dependent diffusion coefficient. This diffusion term means

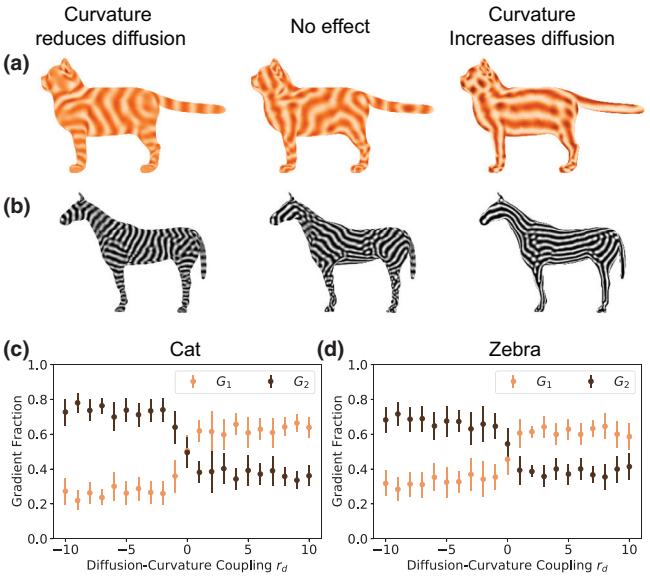

FIG. 3. Diffusion coupled to curvature gives robust alignment on curved surfaces. (a), (b) Simulation results of the Schnakenberg equations on 3D models of (a), a cat and (b), a zebra for different curvature-diffusion coupling strengths, $r_d = -10$, $r_d = 0$, and $r_d = 10$ from left to right. (c), (d) Gradient fraction in directions of principle curvature, $\mathbf{t}_1$ and $\mathbf{t}_2$ for $\mathbf{t}_1$, for (c) cats and (d) zebras. Dots show the mean and standard deviation over 10 simulations.

that when the gradient of v is only in the $\mathbf{t}_i$ direction then it diffuses with rate $d(\kappa_i)$.

To test the idea of curvature-dependent diffusion aligning patterns, we chose a simple monotonic diffusion coefficient in the form of a logistic function

$$d(\kappa) = d_0\left(\frac{1}{2} + \frac{1}{1+e^{-\kappa r_d}}\right), \tag{13}$$

where d_0 is the diffusion coefficient at zero curvature, and r_d is the curvature-diffusion coupling strength. The choice of a monotonic function ensures that diffusion is always highest, or lowest, in the direction of highest curvature and so we should have pattern alignment either parallel or perpendicular to it. For positive r_d, curvature increases the diffusion coefficient and we expect stripes to align perpendicular to the direction of highest curvature. For negative r_d, diffusion decreases with curvature, and stripes should align parallel to the direction of curvature. Additionally, stripe width will depend on curvature, since increasing diffusion increases the pattern wave length [Fig. 1(d)]. For negative r_d, we expect smaller stripes around highly curved regions such as the legs and tail when compared to less curved regions such as the torso.

We simulated curvature-coupled Schnakenberg equations on meshes of a cat and a horse. The surface curvature is calculated using the pymeshlab package in python, and simulations are numerically integrated using the fipy package [30]. Starting from a uniform steady state plus some noise, we evolve the equations until a steady state pattern is reached.

For no curvature coupling, $r_d = 0$, we observe stripe formation with no clear preferred orientation around the torso, legs, or neck [Figs. 3(a) and 3(b), middle]. Around the tails the stripes align with the curvature, likely due to the radius of

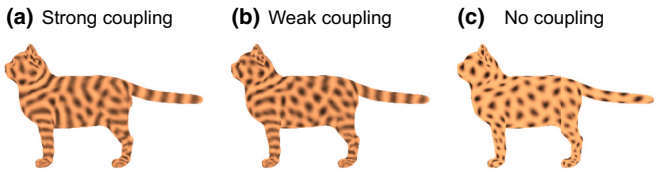

FIG. 4. Diffusion coupled to curvature can drive spot to stripe transitions. (a)–(c) Images show simulation results for (a) strong curvature coupling ($r_d = -10$), (b) weak curvature coupling ($r_d = -5$), and (c) no curvature coupling ($r_d = 0$).

curvature being smaller than the typical wave size, and so it is unable to form a gradient in that direction [4,17].

For negative curvature coupling, $r_d < 0$, meaning diffusion is lower in the direction of highest curvature, we find patterns similar to those observed in tigers and zebras [Figs. 3(a) and 3(b), left]. Along the neck and torso of the animals the stripes are vertical, since they align with the curvature. Along the legs the stripes are instead horizontal and have a smaller wavelength than the torso, also seen in nature. In contrast, for positive curvature coupling, $r_d > 0$, stripes align perpendicular to the direction of highest curvature, resulting in horizontal stripes along its torso, more like a zebrafish than a zebra [Figs. 3(a) and 3(b), right]. Additionally, despite the small circumference of the tail, a single horizontal stripe is able to form, running the length of the tail.

To quantify the effect of curvature coupling, we perform a similar analysis to the flat case, in which we define the gradient fraction in the direction of principal curvatures, $\mathbf{t}_i$, by

$$G_i = \frac{\int (\mathbf{t}_i \cdot \nabla_S u)^2 dS}{\int (\nabla_S u)^2 dS}. \tag{14}$$

For both the cat and zebra models, we find that for negative coupling, $r_d < 0$, the gradient mostly aligns perpendicular to the direction of highest curvature, $\mathbf{t}_1$, forming stripes aligned with curvature [Figs. 3(c) and 3(d)], while for positive coupling the trend is reversed. When the coupling is close to zero, the strength of orientation becomes weaker and the gradient fractions approach a value of $1/2$.

Finally, we perform simulations with the spot-forming parameters with curvature-dependent diffusion. For zero coupling, we obtain the expected uniform spot patterns, even along the tail and legs [Fig. 4(c)]. For weak negative coupling, $r_d = -5$ we observed spots on the torso while stripes form around the tail, neck, and legs of the cat as observed in many spotted cat breeds such tabby cats or Bengal cats [Fig. 4(b)]. For strong negative coupling, $r_d = -10$, we observe mostly stripes on the cat, going around the torso and legs as in regular striped cats [Fig. 4(a)]. For positive coupling, we still observed spotted patterns similar to the case with no coupling. However, this is likely due to the diffusion function used, which has a range between $\frac{1}{2}d_0$ and $\frac{3}{2}d_0$. With a larger range one would expect positive coupling to allow stripes to form, given the analysis in Sec. III.

V. DISCUSSION

In this paper, we have shown how reaction-diffusion systems that form stripes can be oriented by including anisotropic

diffusion (Fig. 1). When the inhibitor diffuses faster in one direction, relative to the activator, then stripes will be formed perpendicular to that direction, even for small differences in diffusion (Fig. 2). Using curvature-dependent diffusion rates, we qualitatively capture the striped patterns observed in many animals (Fig. 3). When curvature decreases diffusion, stripes run around the torso and legs, as observed in zebras and cats. Moreover, a consequence of the decreased diffusion around the legs, relative to the torso, is the reduction of stripe width which is also seen in these animals. In contrast, when curvature increases diffusion, stripes run along the torso and down the legs. Additionally, we have shown how anisotropic diffusion can cause a spots to stripes transition, with negative diffusion coupling giving patterns similar to in spotty cats (Fig. 4).

While the curvature-dependent diffusion is purely theoretical, there are several biological candidates that could enable a curvature-dependent diffusion or reaction rates [31–34]. The patterns were simulated on models of adult animals, but for many animals the patterns are set during embryonic development. In cats the pattern appears to form halfway through gestation [25], although by this stage the embryo is already taking a distinct cat shape, with developed legs and tail showing similar directions of greatest curvature, and so one would expect similar patterns from the model [25]. However, the size of the pattern forming skin cells are more comparable to the scale of curvature in the embryo, thus any curvature effects may be more pronounced during development.

Recent work has demonstrated that some morphogen gradients, measured at the apical surface of the cells, are robust to surface curvature, even when the basal surface is unchanged [28]. If another morphogen followed the length of the basal surface, then the morphogens would display different effective diffusion coefficients under curvature. Similarly, patterning of avian feathers can be generated by both the outer most layer of cells and several layers of cells beneath it, which could further increase the effects of curvature on the length scales of patterns [35].

Alternatively, cells can display strong shape anisotoropy, aligned in the direction of highest curvature, which could affect the rate of diffusion in different directions [29]. If diffusion is cell-boundary limited, then having less cells per unit length due to strain induced by the curvature would increase the effective diffusion rate. In contrast, if diffusion is cytoplasm-limited then straining cells has no effect on the effective diffusion rate. If the two interacting species diffused through different mechanisms, then they would experience anisotropic diffusion that would align patterns.

Finally, there are cases where the diffusing species are actually different cell types which crawl across the surface, such as in the patterning of zebrafish [9]. Some cells can exhibit curvotaxis, in which the crawl speeds can be dependent on the local curvature, effectively changing the diffusion rate in different directions when the principal curvatures are different [36,37].

Overall, this work proposes a new coupling between reaction-diffusion models and the system geometry, and applies this to striped pattern formation and orientation, using only information of the local curvature, instead of globally orchestrated parameter gradients [8,11,12,20]. An interesting follow up question would be to study the case where the curvature is influenced by the reaction-diffusion system, for example by activator induced growth. In this case, a feedback loop would exist between the reaction-diffusion system and the system geometry that may result in complex behavior from a simple ruleset.

In addition, this paper focuses on pattern formation on the torso, legs, and tail which have relatively low Gaussian curvature as they are cylinderlike. The Laplacian on the surface becomes anisotropic implicitly when there is nonzero Gaussian curvature. This idea could be further explored in cases where the Gaussian curvature is significant, such as during early embryonic development where animals are bean shaped, with negative curvature on the stomachs and positive on the backs. Many mammals often have a different fur color on their stomachs, so one could try to model this using curvature-dependent diffusion in a pattern forming system.

ACKNOWLEDGMENTS

I thank Pierre Haas and Carl D. Modes for proof reading the manuscript and giving valuable feedback.

[1] A. D. Melin, D. W. Kline, C. Hiramatsu, and T. Caro, PLoS One **11**, e0145679 (2016).
[2] A. I. Dagg, Mammalia **32**, 657 (1968).
[3] A. M. Turing, Bull. Math. Biol. **52**, 153 (1990).
[4] *Mathematical Biology II: Spatial Models and Biomedical Applications*, edited by J. D. Murray, Interdisciplinary Applied Mathematics Vol. 18 (Springer, New York, NY, 2003).
[5] S. Kondo and T. Miura, Science **329**, 1616 (2010).
[6] L. Marcon and J. Sharpe, Curr. Opin. Genet. Dev. **22**, 578 (2012).
[7] S. Kondo and R. Asai, Nature (London) **376**, 765 (1995).
[8] R. Barrio, C. Varea, J. Aragón, and P. Maini, Bull. Math. Biol. **61**, 483 (1999).
[9] A. Nakamasu, G. Takahashi, A. Kanbe, and S. Kondo, Proc. Natl. Acad. Sci. USA **106**, 8429 (2009).
[10] A. Fofonjka and M. C. Milinkovitch, Nat. Commun. **12**, 2433 (2021).
[11] J. Yang and J. Kim, Chaos Solit. Fractals **169**, 113249 (2023).
[12] R. Sheth, L. Marcon, M. F. Bastida, M. Junco, L. Quintana, R. Dahn, M. Kmita, J. Sharpe, and M. A. Ros, Science **338**, 1476 (2012).
[13] P. K. Maini, D. L. BENSON, and J. A. Sherratt, Math. Med. Biol. **9**, 197 (1992).
[14] H.-S. Jung, P. H. Francis-West, R. B. Widelitz, T.-X. Jiang, S. Ting-Berreth, C. Tickle, L. Wolpert, and C.-M. Chuong, Dev. Biol. **196**, 11 (1998).
[15] S. Sick, S. Reinker, J. Timmer, and T. Schlake, Science **314**, 1447 (2006).
[16] P. Müller, K. W. Rogers, B. M. Jordan, J. S. Lee, D. Robson, S. Ramanathan, and A. F. Schier, Science **336**, 721 (2012).

[17] T. Lacalli, D. Wilkinson, and L. Harrison, Development **104**, 105 (1988).
[18] S. Nampoothiri and A. Medhi, arXiv:1705.02119.
[19] T. W. Hiscock and S. G. Megason, Cell Systems **1**, 408 (2015).
[20] T. Glimm, J. Zhang, Y.-Q. Shen, and S. A. Newman, Bull. Math. Biol. **74**, 666 (2012).
[21] H. Shoji, Y. Iwasa, A. Mochizuki, and S. Kondo, J. Theor. Biol. **214**, 549 (2002).
[22] D. M. Busiello, G. Planchon, M. Asllani, T. Carletti, and D. Fanelli, Eur. Phys. J. B **88**, 222 (2015).
[23] A. L. Krause, M. A. Ellis, and R. A. Van Gorder, Bull. Math. Biol. **81**, 759 (2019).
[24] R. Nishide and S. Ishihara, Phys. Rev. Lett. **128**, 224101 (2022).
[25] C. B. Kaelin, K. A. McGowan, and G. S. Barsh, Nat. Commun. **12**, 5127 (2021).
[26] J. Schnakenberg, J. Theor. Biol. **81**, 389 (1979).
[27] G. Diguet, M. Nakayama, S. Tasaki, F. Kato, H. Koibuchi, and T. Uchimoto, Phys. Rev. E **109**, 014213 (2024).
[28] G. Pierini and C. Dahmann, Sci. Rep. **13**, 8454 (2023).
[29] C. Curantz, R. Bailleul, M. Castro-Scherianz, M. Hidalgo, M. Durande, F. Graner, and M. Manceau, PLoS Biol. **20**, e3001807 (2022).
[30] J. E. Guyer, D. Wheeler, and J. A. Warren, Comput. Sci. Eng. **11**, 6 (2009).
[31] A. E. Shyer, T. R. Huycke, C. Lee, L. Mahadevan, and C. J. Tabin, Cell **161**, 569 (2015).
[32] S. J. Callens, R. J. Uyttendaele, L. E. Fratila-Apachitei, and A. A. Zadpoor, Biomaterials **232**, 119739 (2020).
[33] M. Luciano, S.-L. Xue, W. H. De Vos, L. Redondo-Morata, M. Surin, F. Lafont, E. Hannezo, and S. Gabriele, Nat. Phys. **17**, 1382 (2021).
[34] W. Tang, A. Das, A. F. Pegoraro, Y. L. Han, J. Huang, D. A. Roberts, H. Yang, J. J. Fredberg, D. N. Kotton, D. Bi *et al.*, Nat. Phys. **18**, 1371 (2022).
[35] A. E. Shyer, A. R. Rodrigues, G. G. Schroeder, E. Kassianidou, S. Kumar, and R. M. Harland, Science **357**, 811 (2017).
[36] K. H. Song, S. J. Park, D. S. Kim, and J. Doh, Biomaterials **51**, 151 (2015).
[37] L. Pieuchot, J. Marteau, A. Guignandon, T. Dos Santos, I. Brigaud, P.-F. Chauvy, T. Cloatre, A. Ponche, T. Petithory, P. Rougerie *et al.*, Nat. Commun. **9**, 3995 (2018).